Dissolution Patterns and Dispersion in Fractures: Experiments in Radial Geometries

Le XU

Collaborator : Benjy Marks and
P. Szymczak's group
Supervisor: Knut Jørgen Måløy
Co-Supervisors: R.Toussaint and E.G. Flekkøy

"This project has received funding from the European Union's Seventh Framework Programme for research, technological development and demonstration under grant agreement no 316889"

Introduction

Reaction-infiltration instability is a fundamental and important problem in a variety of fields. In geological systems, dissolution plays an important role in the weathering and diagenesis of Earth's rock, dissolution in salt deposits, melt extraction from the mantle.

It is also of fundamental importance in many engineering applications, including dam stability and stimulation of petroleum reservoirs. The important applications in oil industry are to enhance oil and gas production from petroleum reservoirs with optimum injection rate.

Table 1: Experimental works on dissolution process

3D Hassler Cell Coreflood in Porous matrix	2D Hele-Shaw Cell Diskflow in Fracture
Daccord, Lenormand 1987[7] Hoefner, Fogler 1988[12] Wang et al. 1993[28] Frick et al. 1994 [10] Fred, Fogler 1998[9] Tardy et al. 2007 [27] McDuff et al. 2010 [17]	Daccord 1987 (water/gypsum)[6] Golfier et al. 2001(water/salt)[11] Detwiler et al. 2003[8]

Background – Experimental Part

by G.Daccord, 1987 and R.Detwiler, 2003

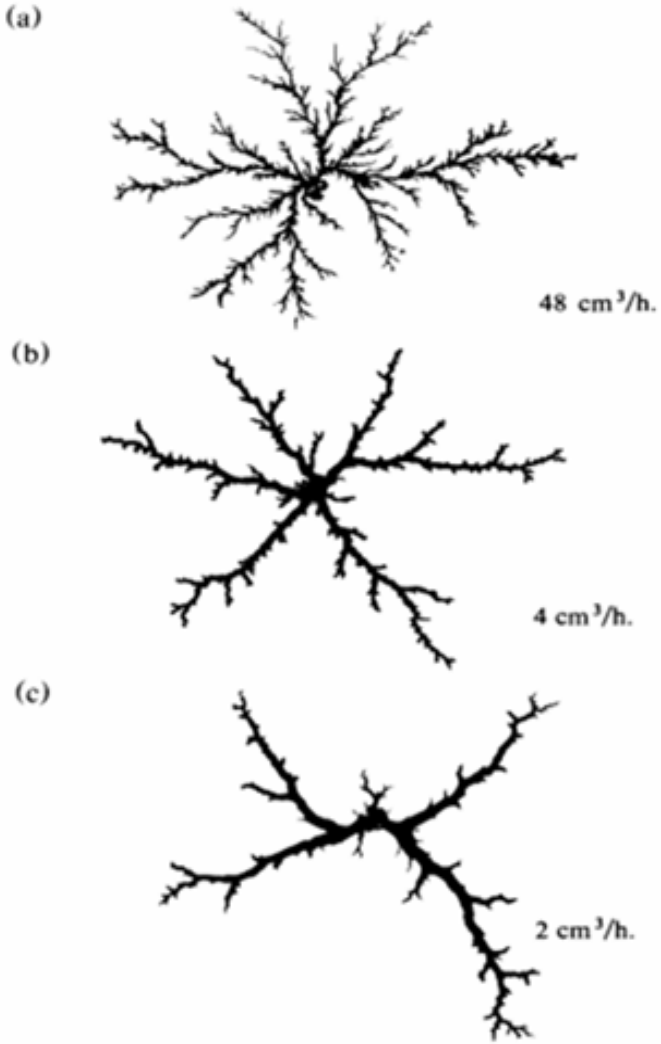

Photographs of 2D radial experiments after 4h and performed at different injection rates. PRL, 1987

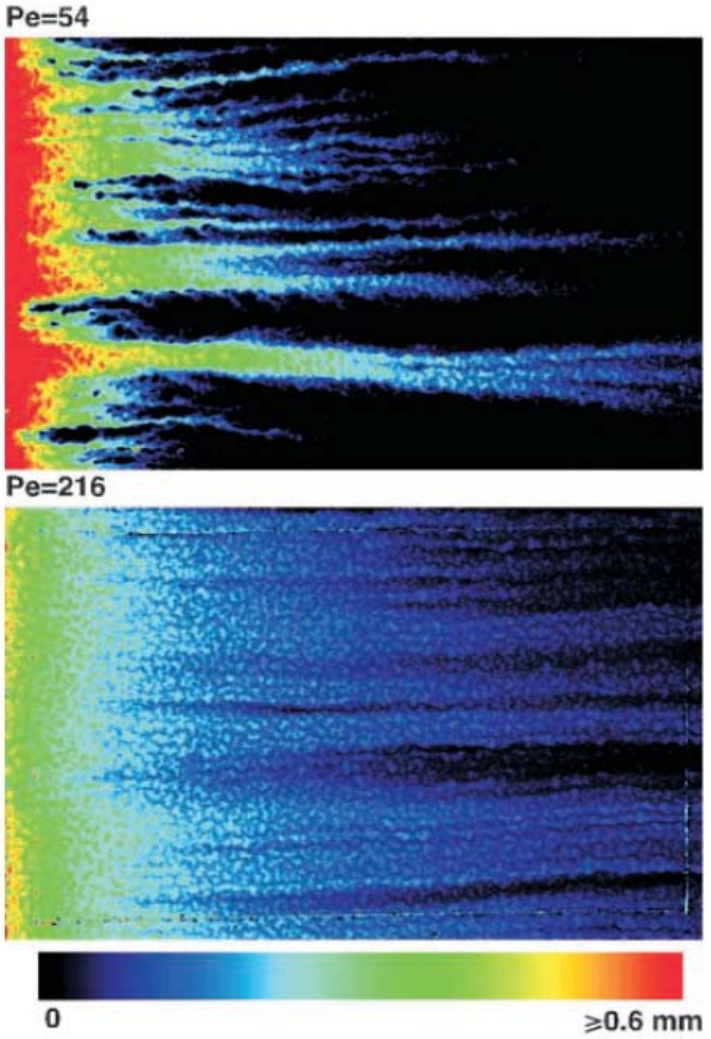

Dissolution-induced aperture growth for the Pe = 54 and 216 experiments, respectively. GRL,2003

Scheme of the Experiment

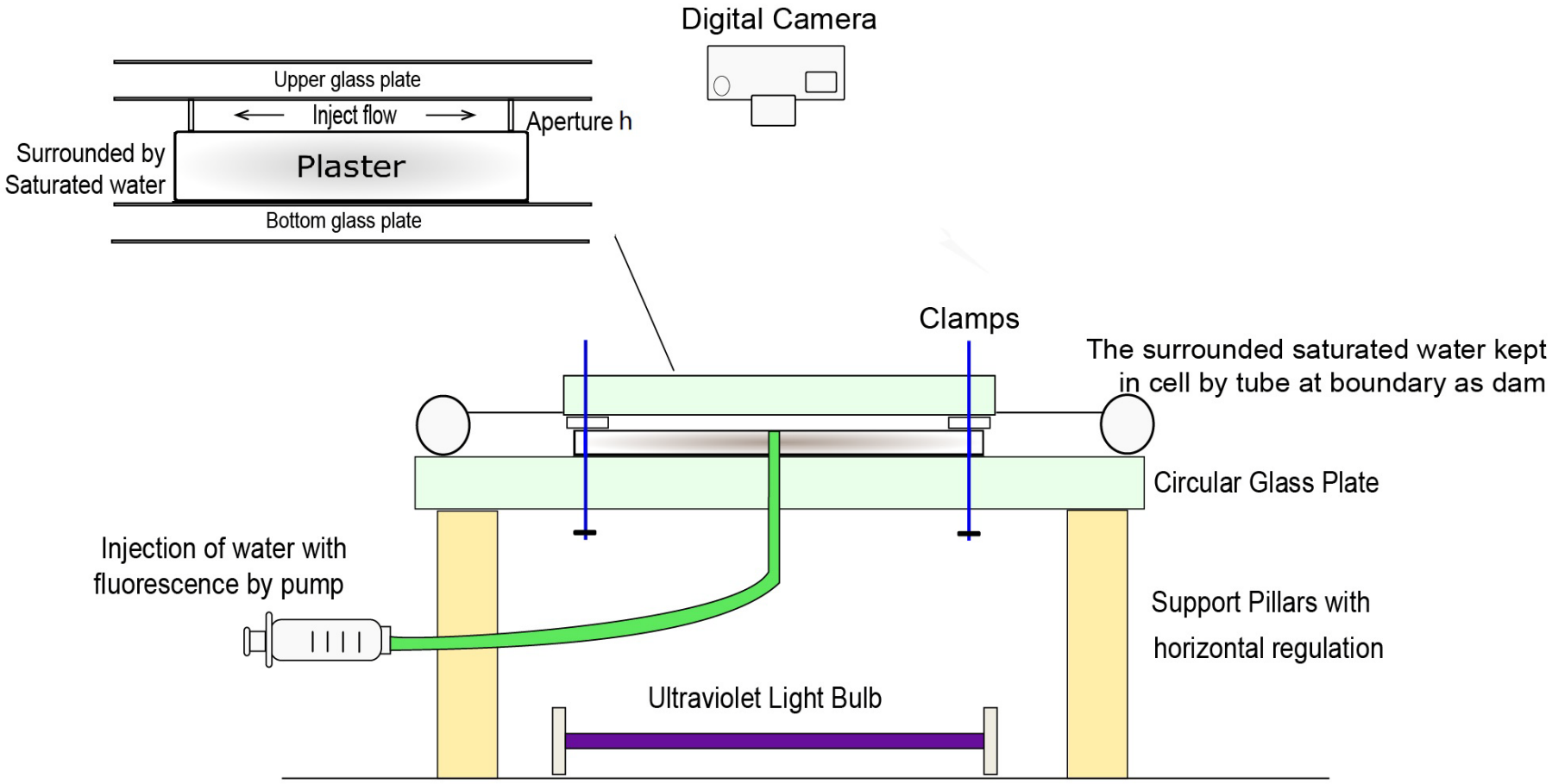

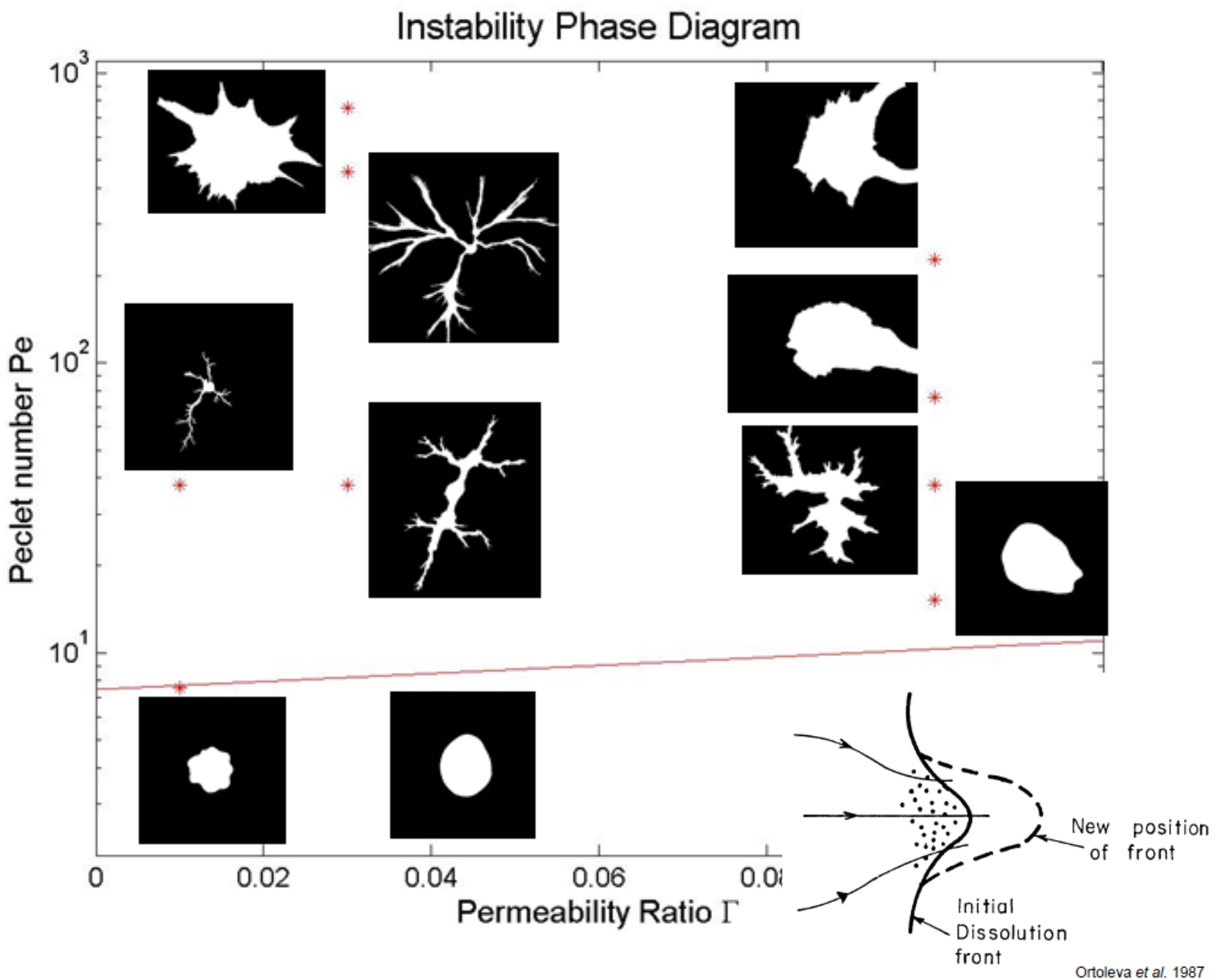

Ortoleva *et al.* 1987

Damköhler number Da and Péclet number Pe

- We conclude that the dissolution pattern related to reaction-infiltration instability is determined by the relation of these 3 process. We can choose 2 dimensionless ratio number to represent these relations, normally they are Damköhler number Da and Péclet number Pe.
- Typically if we draw a dissolution pattern phase diagram with these 2 numbers, all the dissolution situations will be included in this phase diagram.

$$Da = \frac{k(c_{eq} - c)}{u(c_{eq} - c)} = \frac{k}{u} = \frac{kh}{q}$$

$$Pe = \frac{u/h}{(D_m/h^2)} = \frac{uh}{D_m} = \frac{q}{D_m}$$

Variables	Explanation or definition of variables	Units and Reference values
b	Spacing width between two glass plates	$1mm$
h	Fracture aperture	$50/100\mu m$
r_i	Radius of inlet	$7mm$
r_{ext}	Radius of glass plate	$25cm$
ρ	Density of gypsum dihydrate	$2.32g/cm^3$
C	Concentration in solution	$0 - 0.015mol/L$
C_s	Concentration of solid phase	$0.013mol/cm^3$
C_{eq}	Concentration of equilibrium (Solubility)	$0.015mol/L$
s_0	Surface Area Density i.e interfacial area per unit volume of the medium	$10^6 m^2/m^3$
$R(C)$	Reaction rate	$mol \cdot L^{-1}s^{-1}$
$f(C)$	Reactive flux $R(C) = s_0 f(C)$	$mol \cdot m^{-2}s^{-1}$
$k_0 = f(0)$	Initial surface reaction kinetic constant	$3.5 \cdot 10^{-3} molm^{-2}s^{-1}$
k	Dissolution surface reaction rate constant	$2.3 \cdot 10^{-4} m/s$
μ	Viscosity of pure water	$8.9 \cdot 10^{-4} Pas$
κ	Permeability of gypsum	$10^{-13} m^2$
a	Pore Size of gypsum	$10^{-6} m$
φ	Porosity of medium	0.4
D_m	Molecular diffusion coefficient of Calcium in water	$10^{-9} m^2/s$
Q	Injection rate	$0.6/3/12/36/60ml/h$
u_0	Flow velocity at inlet	$1.3/3.9/15.6/26 \cdot 10^{-3} m/s$
Pe	Péclet number	$7.8/39/468/780$
Da	Damköhler number	$0.009/0.015/0.06/0.18/0.3$

Project Framework

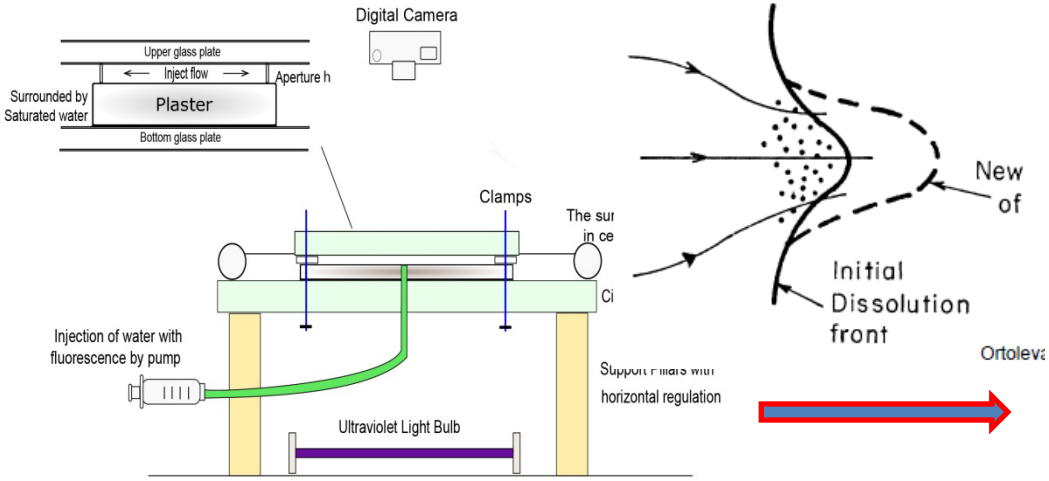

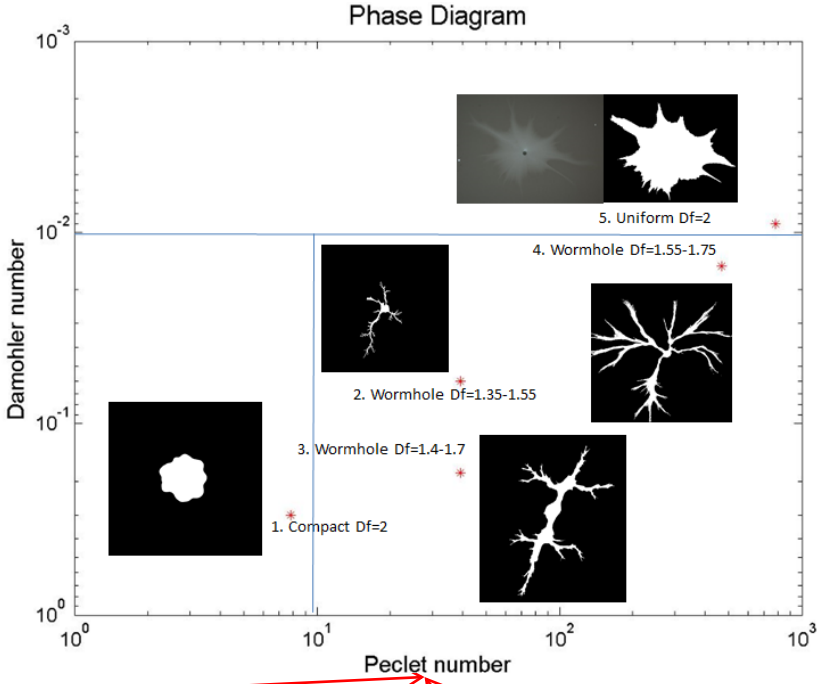

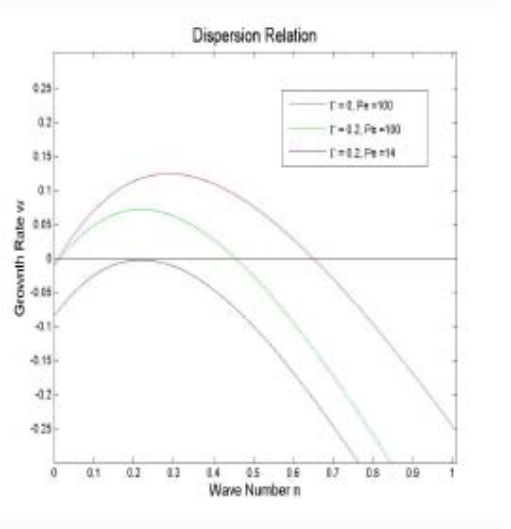

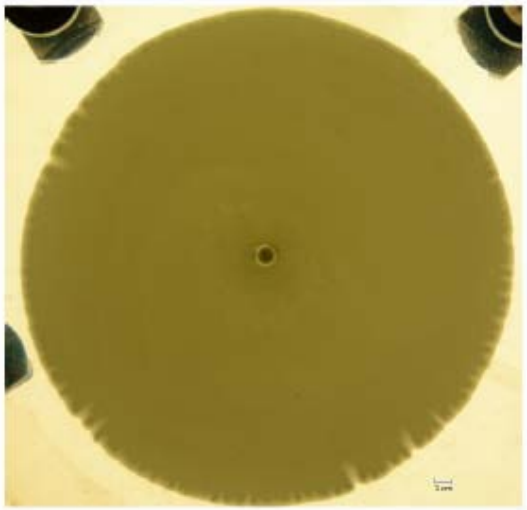

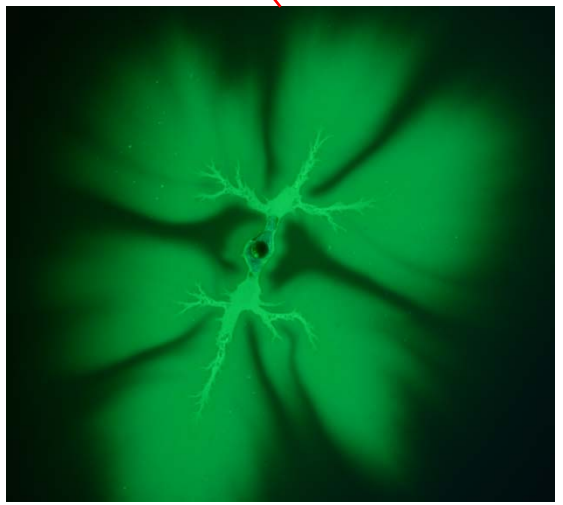

Dispersion Photographs

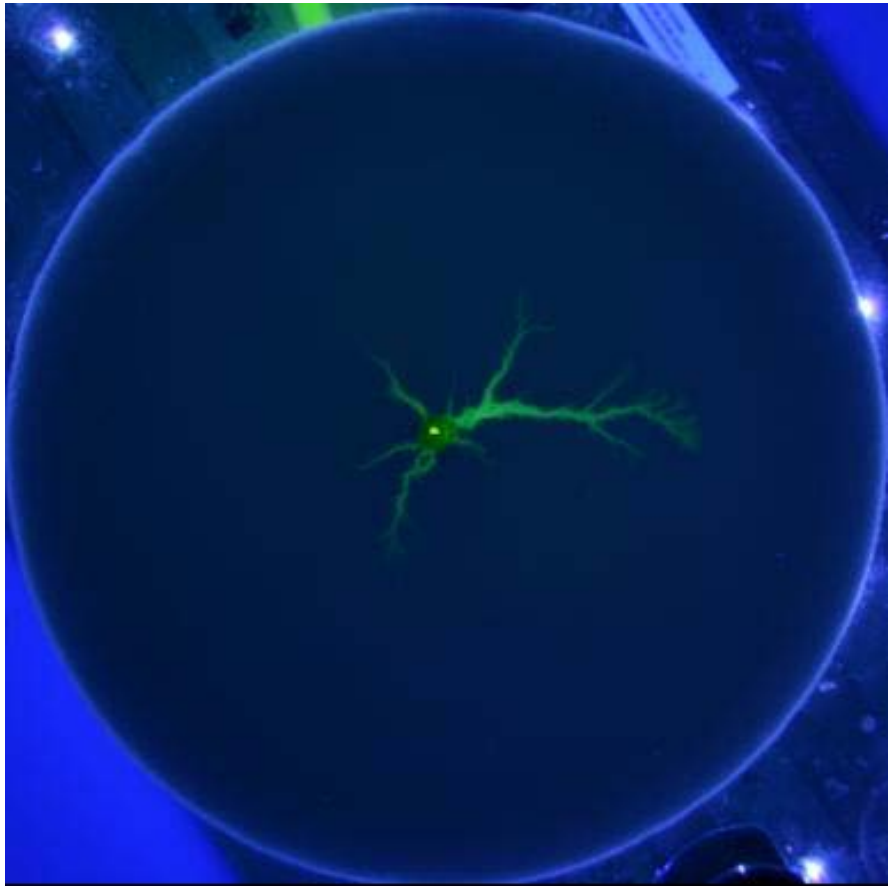

Dispersion Photographs

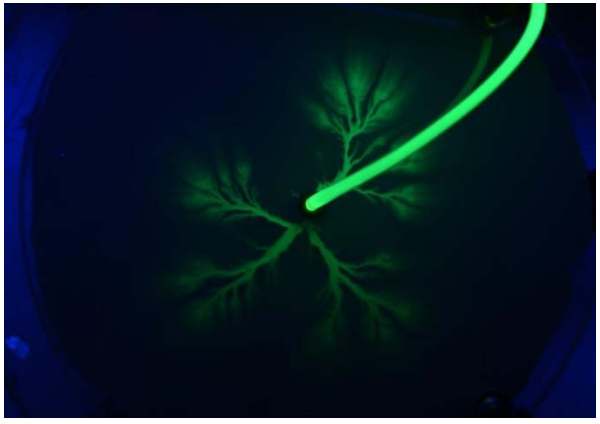

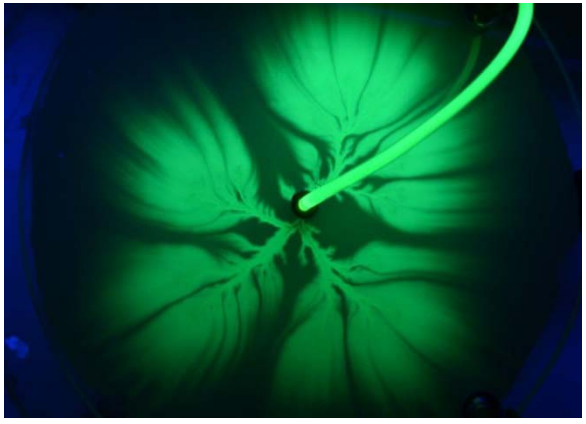

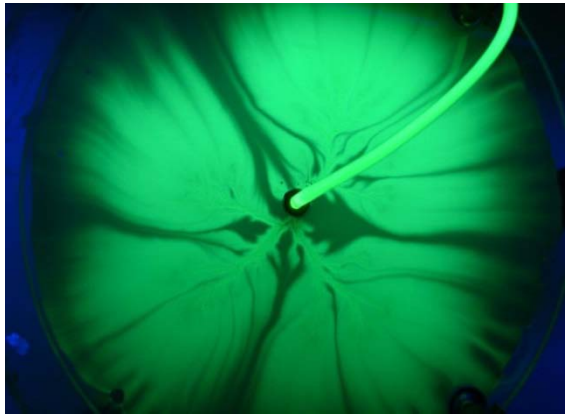

Simulations

$$\begin{cases} Darcy's \quad Law: & \vec{v} = \frac{\vec{q}}{A} = -\frac{\kappa}{\mu}\nabla P \\ Incompressible \quad flow: & \nabla \cdot \vec{v} = 0 \end{cases}$$

Laplace's Equation:

$$\Rightarrow \Delta P = 0$$

Convection-diffusion equation:

$$\frac{\partial c}{\partial t} = \nabla \cdot (D\nabla c) - \nabla \cdot (\vec{v}c) + R$$

D is the diffusivity (diffusion coefficient), or dispersion coefficient more specifically in our case. *R* describes "sources" of the quantity *c*.

The concentration field of flux C(r,t) will simulate the flow transport in the porous media and could be compared with experimental flow transport patterns.

Qualitative Comparison

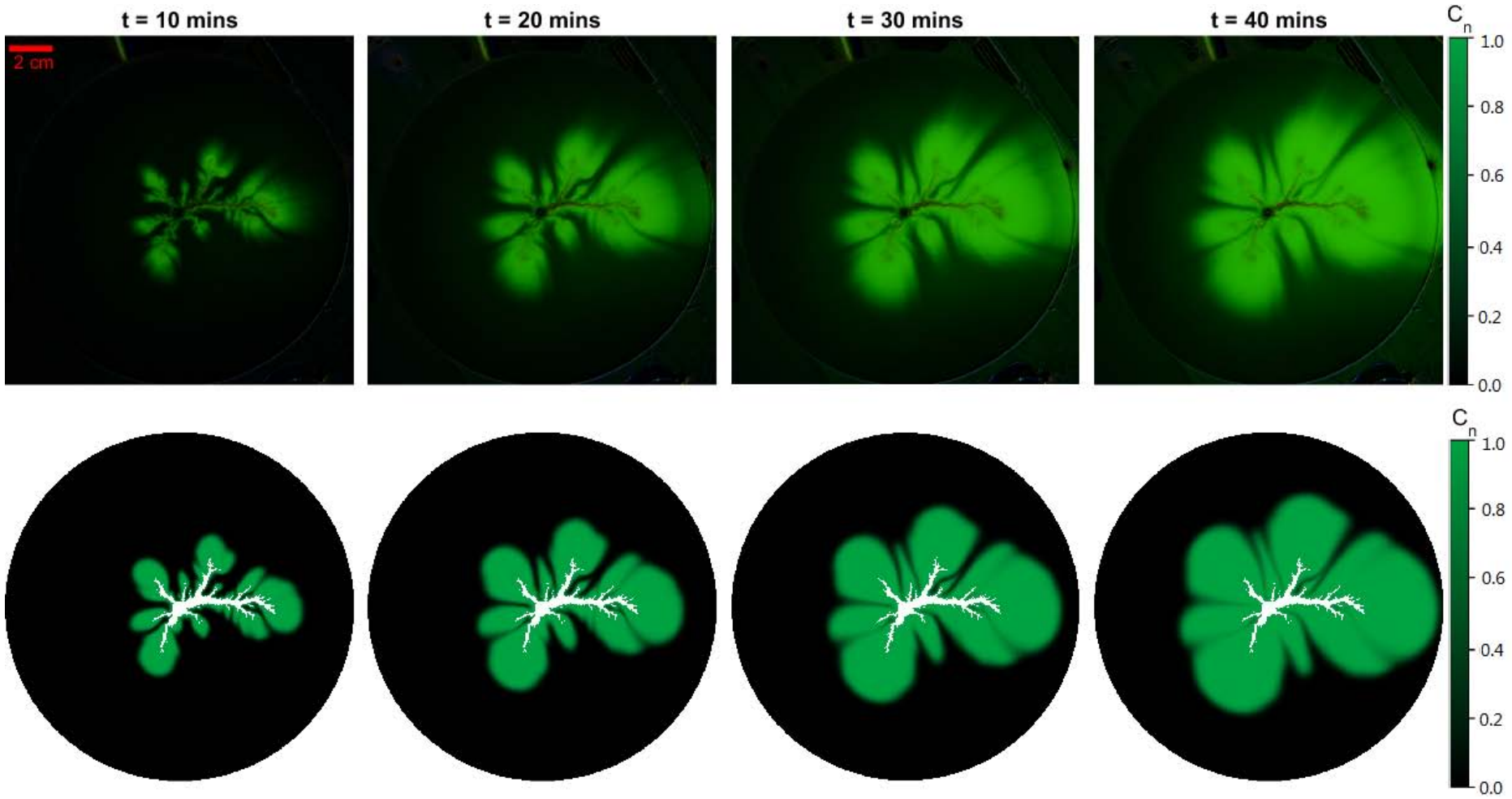

Overlap Ratio

$$\gamma_{OL} = 1 - \frac{\sum_{(i,j)\in\mathcal{A}_D} \|E(i,j) - S(i,j)\|}{\sum_{(i,j)\in\mathcal{A}_D} max(E(i,j), S(i,j))}$$

Experiment Image(E)

|E-S|

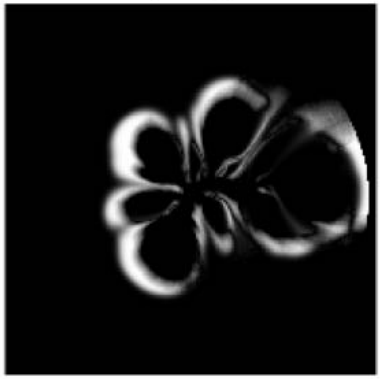

Simulation Image(S)

γ_{SOL} = 0.7297

γ_{IOL} = 0.73806

where E and S are respectively the experimental and the simulation image (i.e. grayscale fields) which have been normalized (i.e. from 0 to 1).
In the case where E and S are binarized (black and white images), this calculation of the overlap ratio leads to the measure of the ratio of the area of intersection between E and S divided by the area of union between E and S

i.e. $A(E \cap S)/A(E \cup S)$

which we call the structure overlap ratio SOL. This computation can also be performed on the gray-scaled images of E and S to obtain the intensity overlap ratio IOL.

Time Evolution

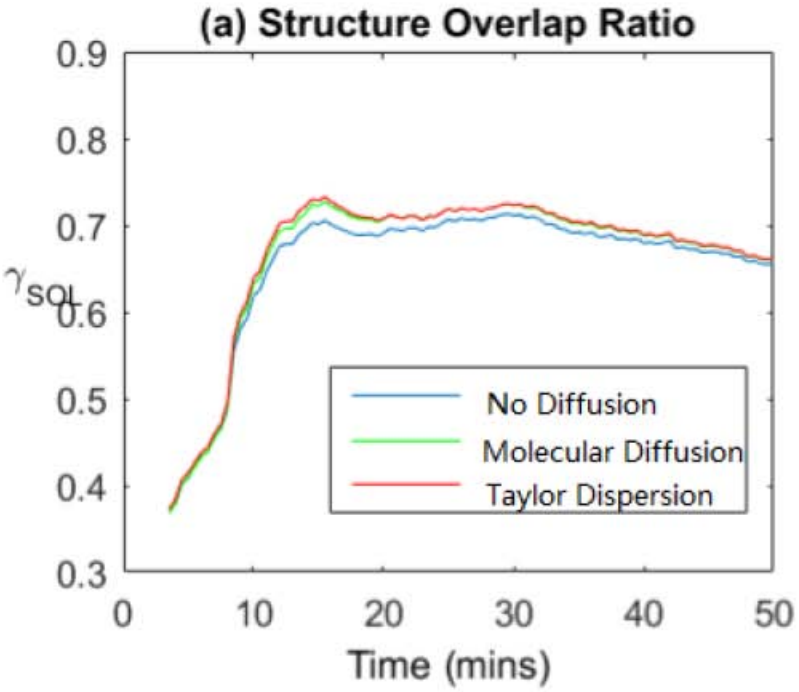

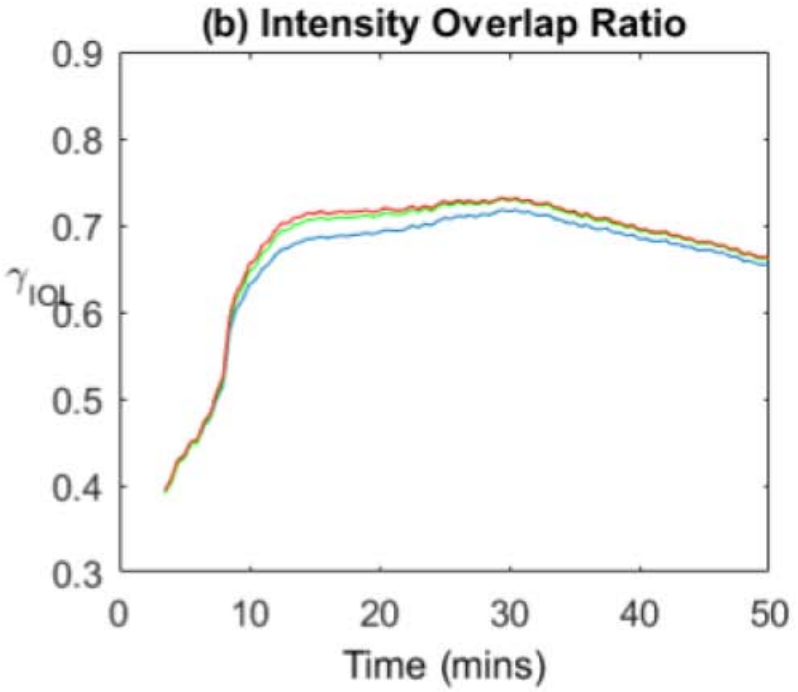

Dynamic process of dispersion: the value of the overlap ratio evolves with time.

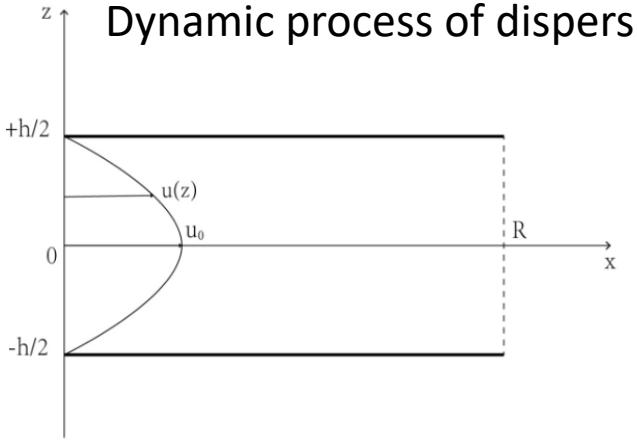

Taylor Dispersion

$$D_{\parallel} = \frac{h^2 u_0^2}{210 D_m} + D_m = D_m(1 + \frac{h^2 u_0^2}{210 D_m^2})$$

Differences Between E and S

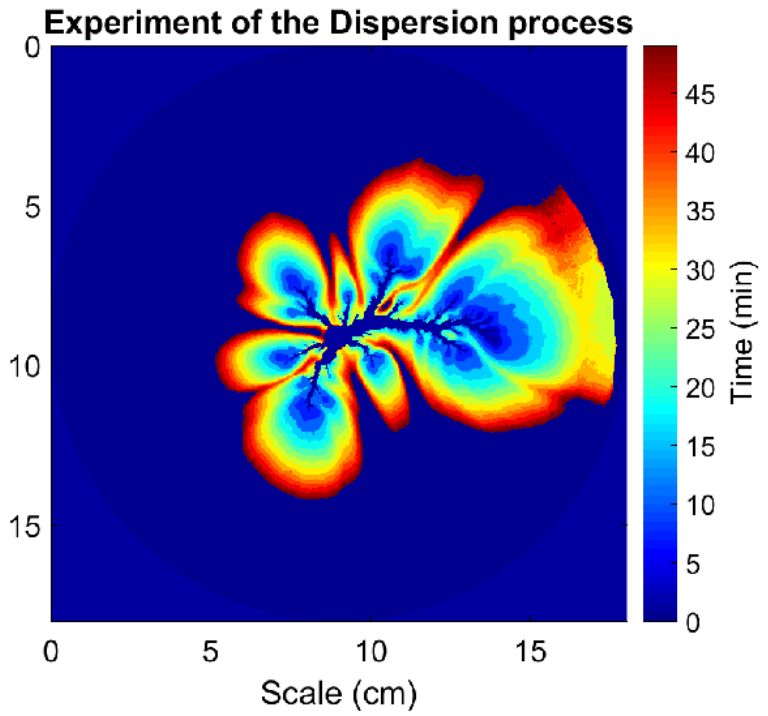

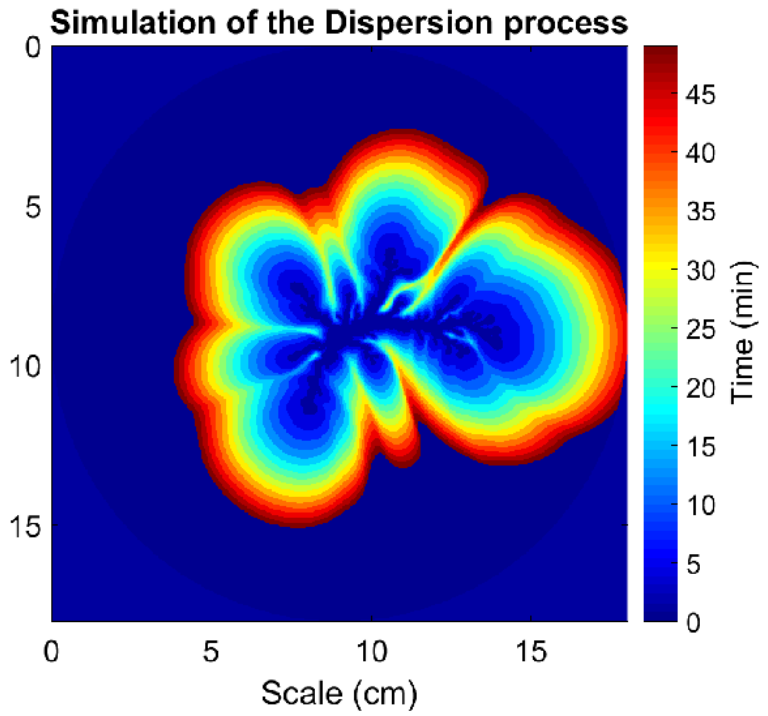

- One reason for this difference is that in the simulations the dissolution patterns are taken to be completely dissolved while in the experiments the plaster sample is gradually dissolved.
- For a similar reason the assumed undissolved part in the simulations might have some dissolved fingers that we are not able to see in the experiments due to limited resolution. These slightly dissolved fingers will give finer scale structures in the dissolution patterns.
- Another difference between the experiments and the simulations is that experimentally, a very small fraction of fluid infiltrates into the porous matrix instead of flowing in the open fracture.

‘Fractal-like’ Pattern

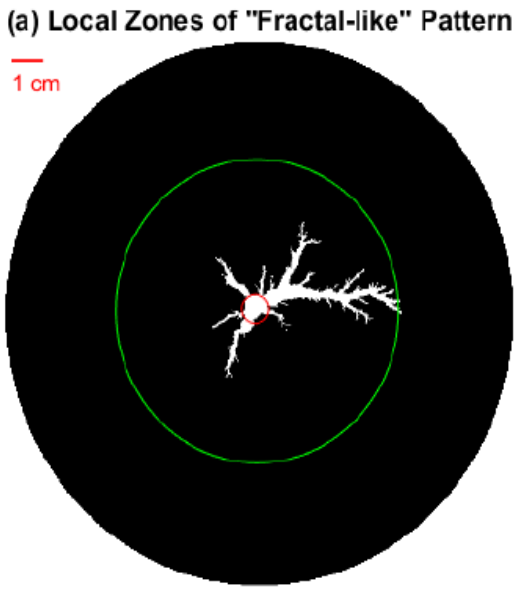

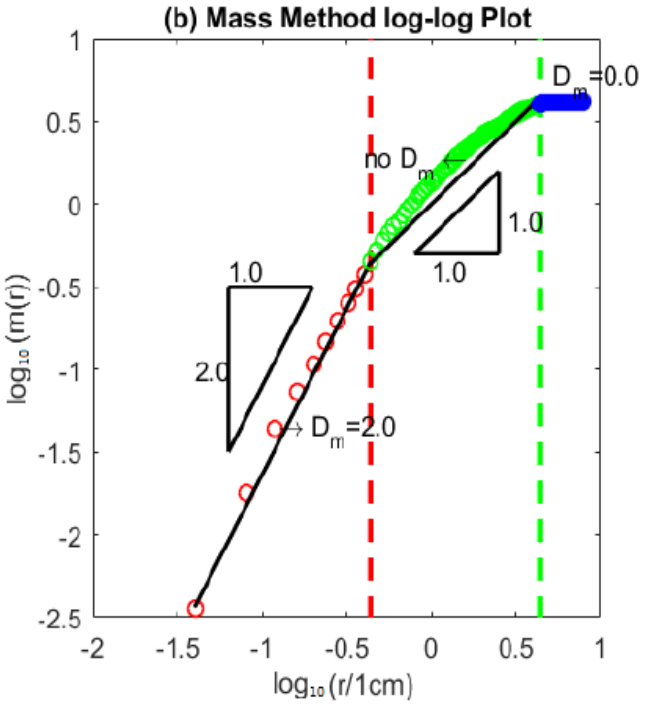

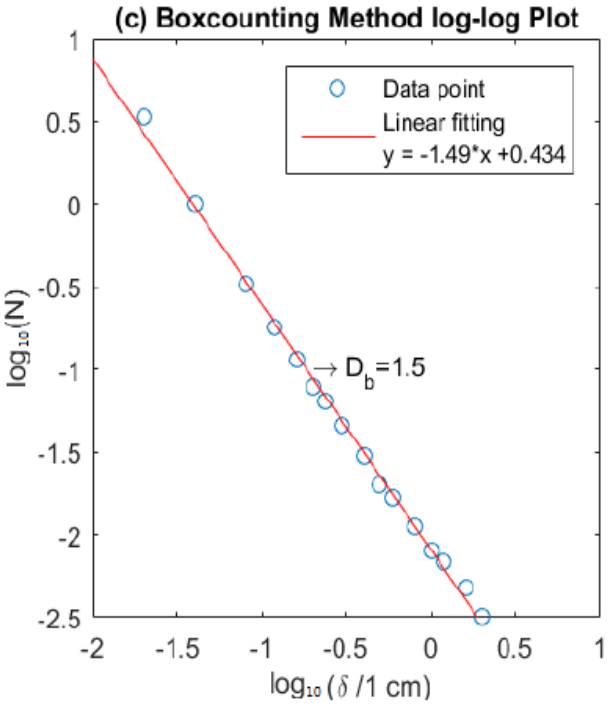

Mass within radius method

$$m(r) \propto r^{D_m}$$

Box counting method

$$N \propto \delta^{-D_b}$$

Concentration Distribution

Ramified Front Simuation(S)

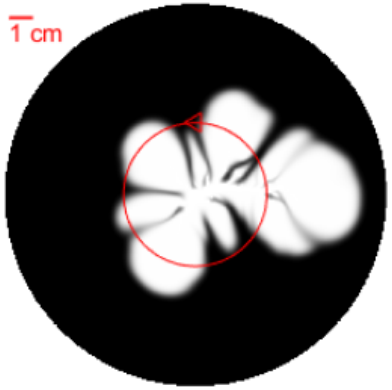

Intensity Distribution at r = 3.4 cm

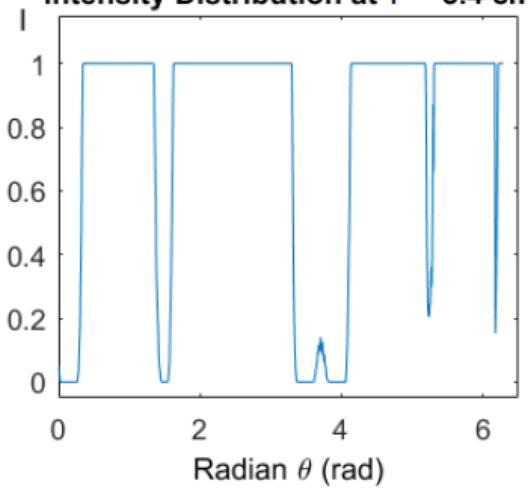

$$< C_n(\mathbf{r}) >= \sum_{i=1}^{N} C_n(\mathbf{r_i})/N(r)$$

Flat Front Simulation (F)

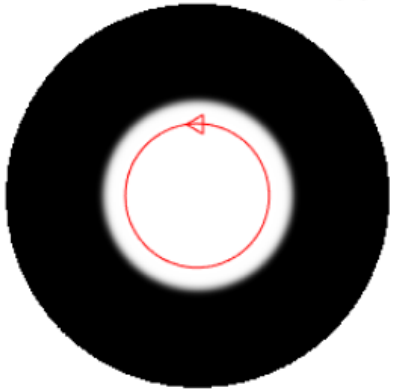

Intensity Distribution at r = 3.4 cm

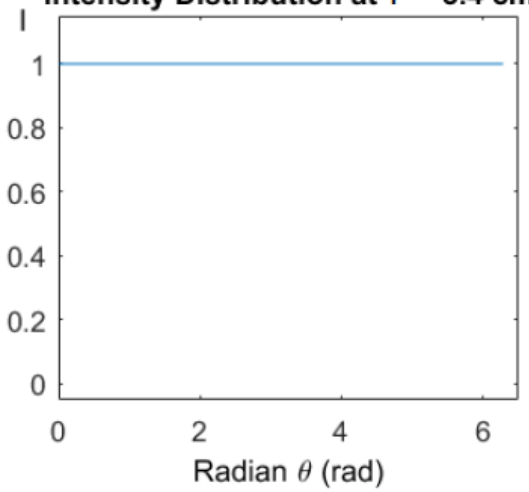

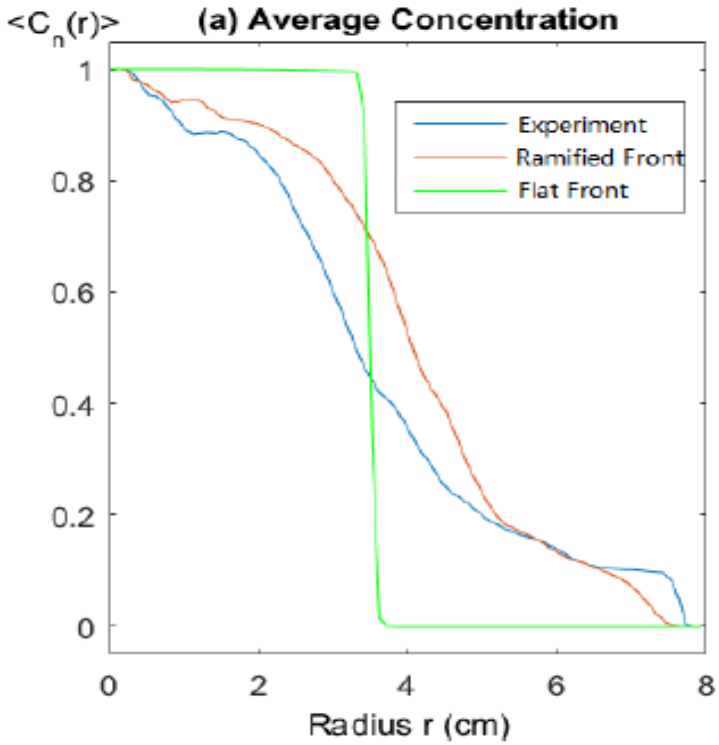

Concentration Distribution Width

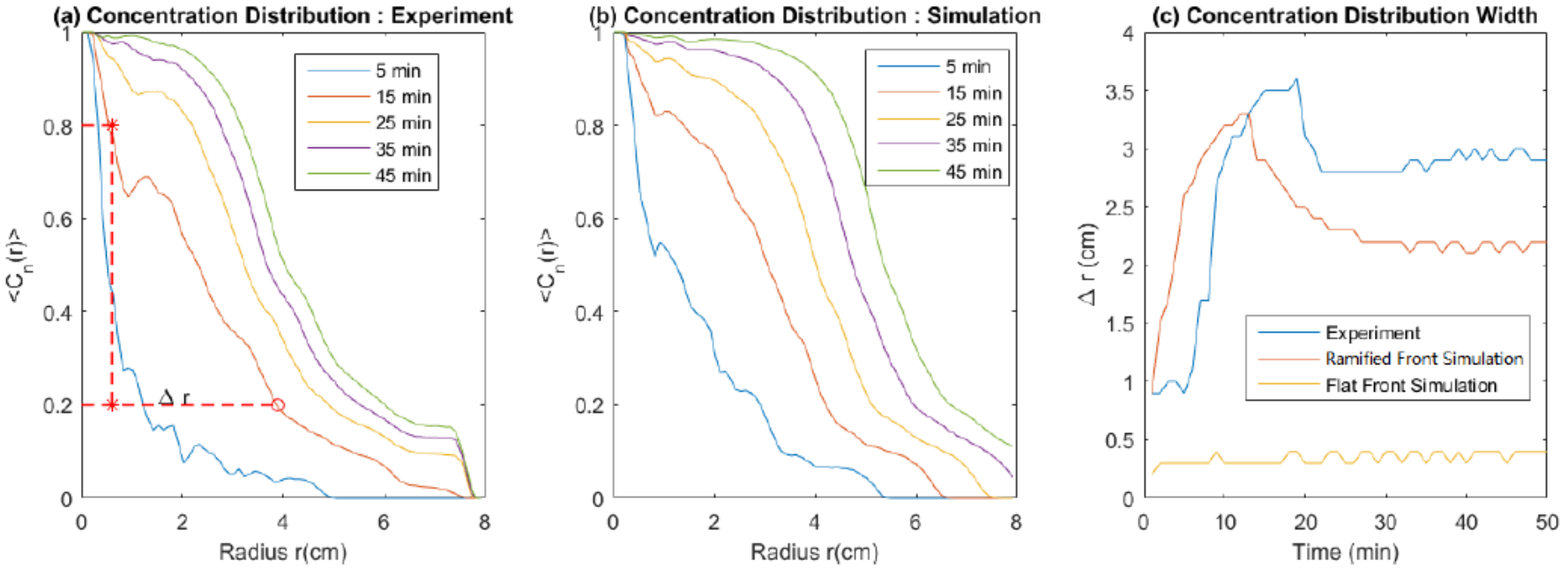

The width of the mean concentration distribution $\Delta r(t)$ in both the experiments and the simulation with ramified initial front increases to a peak and then decreases to a stable value.

An interesting and open question is if these fluctuations will be reduced or disappear for a sufficient large systems and times. Will the model with a circular initial state describe the system at large length scales and times?

Large scale system and long time

$$P(r) = P_0 \frac{\ln(|\mathbf{r} - \mathbf{r}_1|/R) + \ln(|\mathbf{r} + \mathbf{r}_1|/R)}{\ln(a/R)}$$

$$\mathbf{u} = -\kappa \frac{\nabla P}{\mu} = \frac{2\kappa P_0}{\mu \ln(R/a) r} \mathbf{e}_r \left(1 + O\left(\frac{r_1}{r}\right)^2\right)$$

$$\frac{dl_c}{dt} = u(l_C) = \frac{Q}{2\pi l_C h} \qquad l_c = \sqrt{\frac{Qt}{\pi h}}$$

$$\frac{l_{min}}{l_{max}} = \sqrt{\frac{t - t_D}{t}} \approx 1 - \frac{t_D}{2t}$$

$$l_{max} - l_{min} = \sqrt{\frac{Q}{\pi h}}(\sqrt{t} - \sqrt{t - t_D})$$

$$\approx \sqrt{\frac{Q}{\pi h}} \cdot \frac{t_D}{2\sqrt{t}}$$

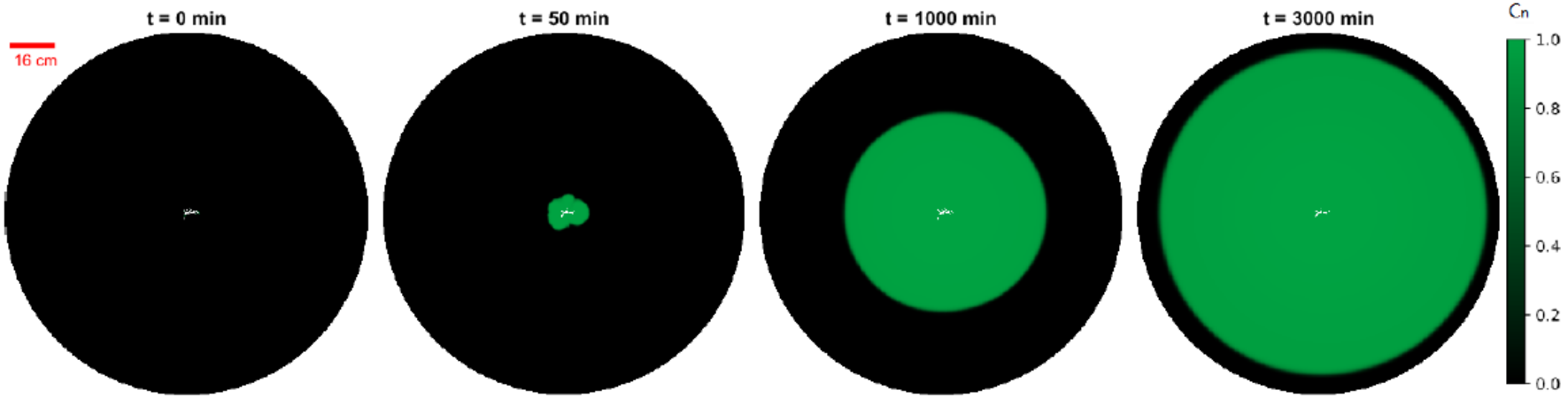

Simulation Compared With Theory

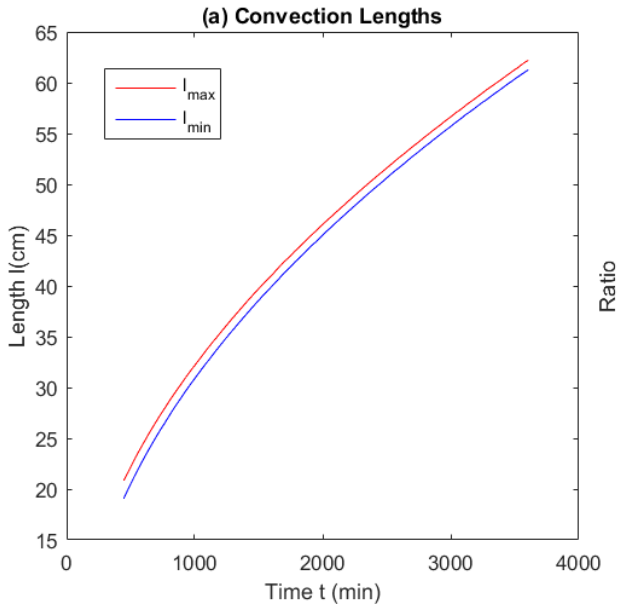

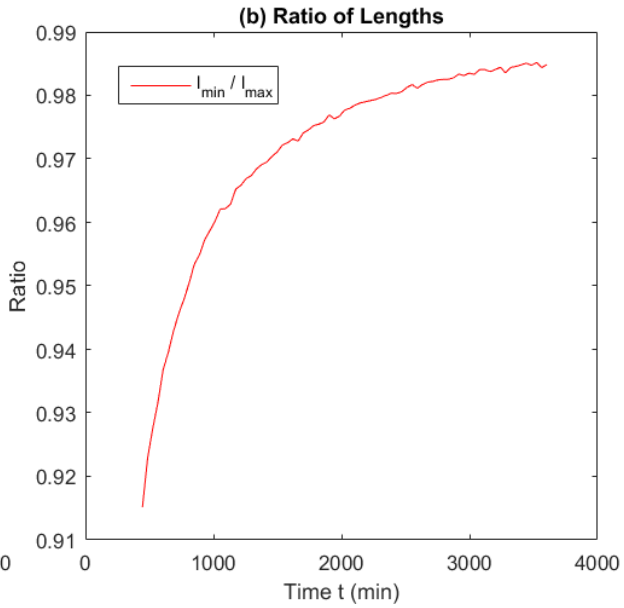

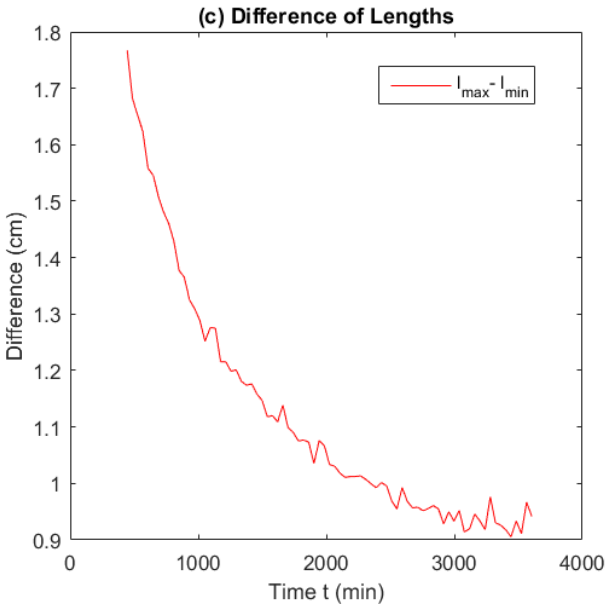

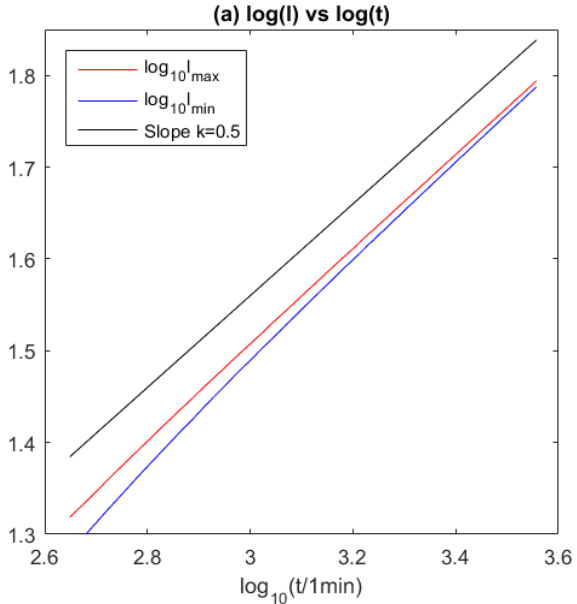

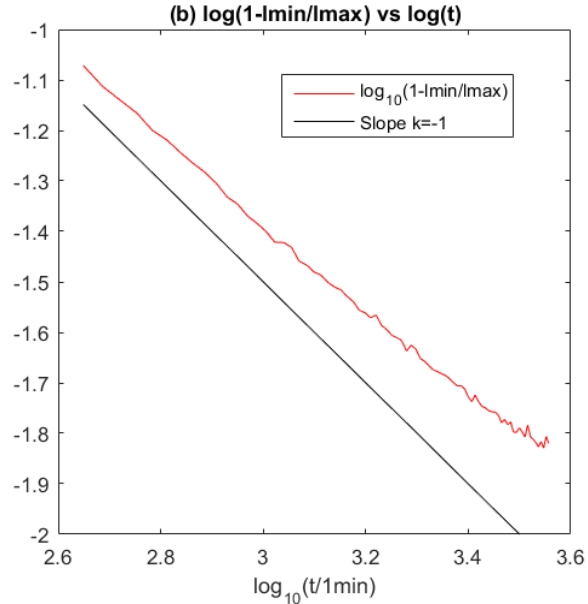

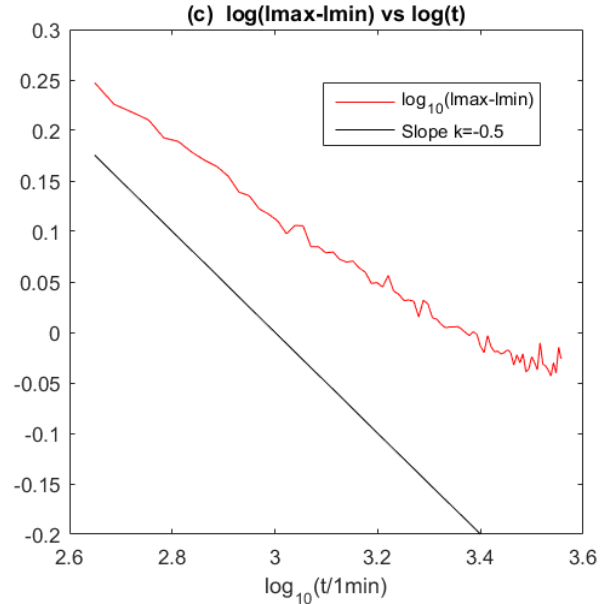

CONCLUSIONS

- For our experiments, simulations with molecular diffusion and Taylor diffusion have no significant difference and show a good similarity with experimental results.
- The ramified dissolution structures turns out to have a significant effect on the local concentration C(r) and the concentration averaged over angles < C(r) > both for small and large length and time scales.
- The shape of concentration distributions far from the dissolution structure is discussed with some theoretical calculations. And the results are confirmed by the simulation in large scale system.

OUTLOOK

- At the expected 3D structure, we predict that the shape of concentration distribution far from the dissolution structure will eventually experience a slowly vanishing anisotropy, it would certainly be nice to explore these structures both experimentally and numerically to see how they correspond to these predictions in future work.

Thank You For Listening

ACKNOWLEDGMENTS

This project has received funding from the European Union's Seventh Framework Programme for research, technological development and demonstration under grant agreement no 316889. We acknowledge the support of the University of Oslo and the support by the Research Council of Norway through its Centres of Excellence funding scheme, project number 262644, and the INSU ALEAS program. We thank Mihailo Jankov for technical support and Marcel Moura, Fredrik K.Eriksen, Monem Ayaz and Guillaume Dumazer for useful discussions.